

Novel Approach to Constructing an Ultra Low Cost Flowcell Biosensor

THESIS

Presented to the Faculty of the Department of Physics and Astronomy
in Partial Fulfillment of the Major Requirements
for the Degree of

BACHELOR OF SCIENCE IN
PHYSICS

Jeffery Summers

May 2019

©2019 Middle Tennessee State University

All rights reserved.

The author hereby grants to MTSU permission to reproduce
and to distribute publicly paper and electronic
copies of this thesis document in whole or in part
in any medium now known or hereafter created.

Novel Approach to Constructing an Ultra Low Cost Flowcell Biosensor

Jeffery Summers

Signature of Author:

Department of Physics & Astronomy

May 2019

Certified by:

Dr. William Robertson

Department of Physics & Astronomy

Thesis Supervisor

Accepted by:

Dr. Ronald Henderson

Professor of Physics & Astronomy

Chair, Physics & Astronomy

ABSTRACT

In this thesis we present our approach to constructing an ultra low-cost flowcell biosensor. Our sensor is capable of detecting changes in index of refraction on the order of 10^{-3} , showing that it is well suited for not only index testing but also for surface loading processes where binding between molecules may occur. Our sensor utilizes 3D printed parts, a one dimensional photonic crystal coupled to a glass prism (rather than a traditional SPR metal-film-prism coupling system), and a CCD to operate. Highly sensitive Bloch Surface Waves (BSWs) can be excited in the outer layer of our multilayer by coupling an incident laser beam to the prism-multilayer structure and the position of the BSWs can be tracked by analyzing the reflected beam. By using this method we are able to bring the cost of manufacturing the sensor to about \$100, excluding the photonic crystals which can be fabricated commercially. The majority of our expenses come from a CCD chip and a neutral density filter ($d=3.5$).

TABLE OF CONTENTS

Abstract	iii
I. Introduction	1
II. Experimental Design	4
III. Methods	8
IV. Results	11
V. Conclusion	14
VI. References	15

LIST OF FIGURES

1	Surface Plasmon Resonance setup	1
2	The laser on the right side of the image couples into the prism-multilayer structure atop the centerpiece and is then reflected into a CCD where data can be taken.	2
3	An illustration of the photonic crystal used in our sensor	4
4	Top: the beam holding the laser and focusing lens. Bottom: the beam holding the camera and neutral density filter.	4
5	Primary stage and flowcell stage of our sensor. The green round 3D printed fixture underneath the flowcell is the primary stage which the two beams are attached to via a small divot in the back. The blue 3D printed piece mounted to the primary stage is the flowcell stage. The glass prism, multilayer, and flowcell chamber are attached atop the flowcell stage with the use of hex screws and 3D printed braces.	5
6	The flowcell stage, prism, multilayer and flowcell chamber. A rubber gasket is set in a groove around the chamber so that when the braces are tightened the interface between the multilayer and flowcell is liquid tight.	6
7	The geometry behind our coupling angle when the flowcell chamber is filled with water. The lines normal to the left leg and hypotenuse of the triangle represent the surface normals of the prism. The line 40° from the left leg surface normal and 66° from the hypotenusal surface normal represent the path of the incident light. The laser needs to be oriented about 5° off of parallel with the hypotenusal face of our prism. It is quite an awkward angle, but a different flowcell stage can be printed to make reaching this coupling angle more natural by translating the prism's bed upward.	7
8	The reflectance characteristic of our multilayer. This plot was developed using a transfer matrix method.	8
9	The theoretical relation between the angular position of the mode and the index of refraction inside the flowcell chamber.	10
10	Index shift measurements for ethanol.	11
11	Index shift measurements for acetone.	12
12	Index shift measurements for 70% isopropyl alcohol.	12
13	Plotted above is the relationship between a shift in the mode position (measured in pixels) and a shift in the index of refraction of the chamber, δn_c	13

I. INTRODUCTION

Flowcell sensors have many applications; disease detection, refractive index measurements and measurements of reactivity to name a few [1]. These sensors have been operating on the basis of electromagnetic surface phenomena for decades [1]. Most flowcells on the market work by exploiting surface plasma oscillations (SPOs). These oscillations are highly sensitive to changes in the optical properties of the adjacent medium and follow from Maxwell's equations when the dielectric functions of each medium satisfy the relation below [2, 3, 4].

$$\frac{\epsilon_{spo}}{\epsilon_{adjacent}} < -1$$

Metals like aluminum, copper, gold, and silver have negative dielectric functions at wavelengths in the red/infrared [2], so films of these metals are used to generate SPOs in most flowcell sensors via a process known as Surface Plasmon Resonance (SPR) [1]. An SPR system utilizes light-prism coupling to excite the surface electrons on a thin metal film deposited on the hypotenusal face of the prism. A dark band representing the photons coupled

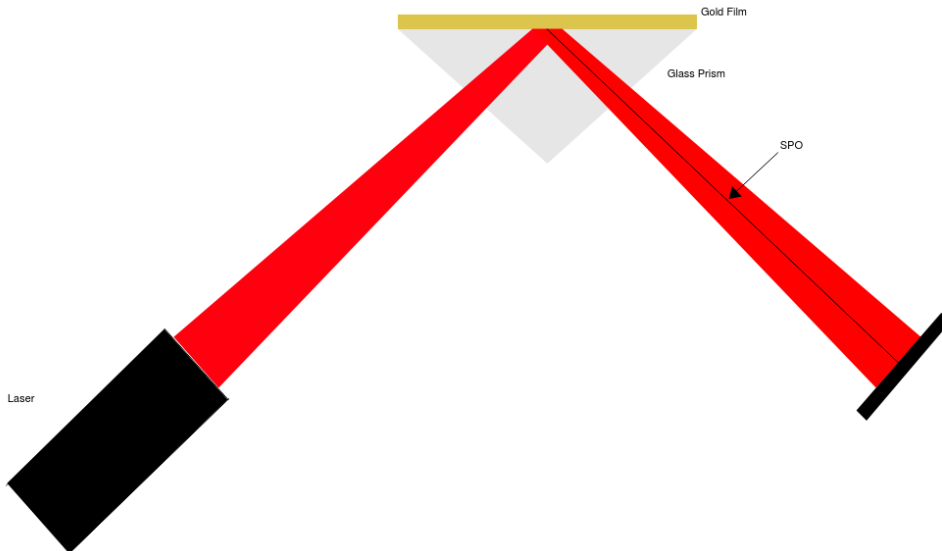


Figure 1: Surface Plasmon Resonance setup

into the surface wave appears on the reflected beam image as seen in Figure 1. There are quite a few drawbacks for using metal films, however. Metals are highly reactive so each time an SPR system is used for surface loading processes a new prism must be used. These films also require particular wavelengths of incident light to excite the oscillations. Rather than using metal films, one-dimensional photonic crystals, or multilayers, can be designed to exhibit the phenomenon of surface electromagnetic waves (SEWs) or Bloch surface waves (BSWs), named after the physicist Felix Bloch who was famous for working with periodic systems. The reason for naming them after Bloch is

that these surface waves have (so far) only been generated in photonic crystals which are periodically stratified dielectric stacks. These surface waves have the same practical application as SPOs. Multilayers overcome both of the shortcomings of metal films listed here. They can be designed to work for any wavelength and are typically made of nonreactive glass [2]. Modular 3-D printed parts synthesize nicely with the flexible nature of multilayers, resulting in a sensor that is capable of working with many materials. In addition to these benefits, we expect that our 3-D printed and multilayer-based flowcell sensor will be more sensitive and precise with its measurements [5] and be far cheaper to both build and maintain compared to traditional SPR sensors.

To take measurements with our sensor we look at the reflected image of incident laser light which has been coupled into the prism-multilayer interface to produce a BSW in the terminating layer. Our multilayer is designed to trap incident light in the last layer at a special *coupling angle*; this results in a dark band in our reflected image which essentially tracks the position of the surface mode and is highly sensitive to changes in refractive index and any molecular binding that could take place on the interface. A top-down view diagram of the sensor is shown in Figure 2.

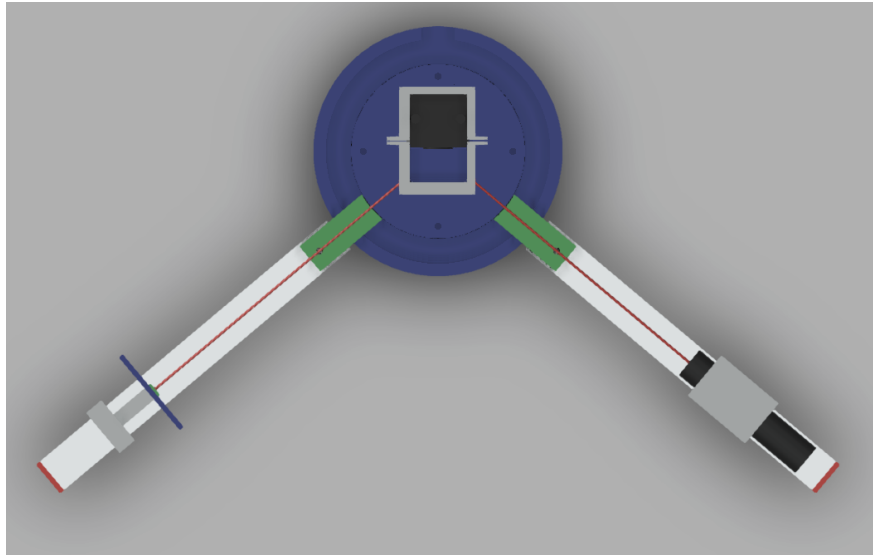


Figure 2: The laser on the right side of the image couples into the prism-multilayer structure atop the centerpiece and is then reflected into a CCD where data can be taken.

As fluids or gases are put into the flowcell chamber the refractive index of the chamber, n_c , changes. The following example provides some intuition as to how the sensor operates, but keep in mind that it is not reflective of how our sensor actually works as we are dealing with a photonic crystal composed of many layers, not just a single interface.

The condition for total internal reflection, found from Snell's law, for the interface between a glass prism (with refractive index n_g) and some transmitting medium whose index of refraction varies with time is given by:

$$\sin(\theta_c(t)) = \frac{n_c(t)}{n_g}$$

Note that the critical angle above is the angle at which a plane wave is incident upon an interface and by the law of reflection it is equivalent to the angle at which the reflected plane wave propagates from the normal of the interface. In this way we obtain an expression for the angle of reflection as a function of time:

$$\theta_r(t) = \arcsin \frac{n_c(t)}{n_g}$$

Again, this expression is only valid for a single interface and hence does not accurately reflect our setup as we use a multilayer that behaves much differently than a single interface. With that said, this expression for θ_r does capture the essence of our setup; the reflected angle (this is equivalent to the position of the surface mode) is dependent on the index of refraction of the chamber. Using this fact we can associate variations in the flowcell chamber's refractive index with differences in the BSWs angular position. These angular differences can be calculated by tracking the variation in the position of the dark band in the reflected image on a CCD. A detailed analysis relating a shift in pixels on the CCD to the angular variation of the surface mode is listed in the section III.

To use this device for disease detection, or to detect any sort of molecular binding process, the multilayer must have a receptor deposited onto the outer layer. The characteristic of the surface mode is first captured with just receptor and a flowcell chamber filled with an inert liquid. After acquiring the characteristic of the surface mode the binding agent is then flushed through the chamber and if binding occurs the surface mode's characteristics will be different than before once the chamber is flushed again with the inert liquid. Once a steady state is reached evidence of binding is given by a changed characteristic of the image of the surface mode.

II. Experimental Design

The process of design for this experiment relies heavily on the use of a 15 millimeter right prism and our photonic crystal. The photonic crystal is composed of 3 bilayers of TiO₂ and SiO₂. The dielectric function of TiO₂ is taken as $\epsilon_{TiO_2} = 4.84 + 0.0007i$ and the dielectric function of SiO₂ is taken as $\epsilon_{SiO_2} = 2.1316 + 0.0001i$. It should be noted that the imaginary parts of each dielectric function may not be accurate due to the values being not well known and have been included to introduce some form of loss that fits the results of prior experiments. Figure 3 illustrates the structure of the multilayer.

The sensor is composed of three different parts: the primary stage, two beams, and the flowcell stage. One of the two beams holds our laser and a focusing lens while the other holds the CCD and captures the reflected beam. Normally the laser light is too intense to pick up the surface mode in the reflected image. We attach a neutral density filter ($d=3.5$, see Figure 4) to the CCD to reduce the intensity and this allows us to image the surface mode.

410.0nm SiO ₂
121.0nm TiO ₂
188.3nm SiO ₂
121.0nm TiO ₂
188.3nm SiO ₂
121.0nm TiO ₂
188.3nm SiO ₂

Figure 3: An illustration of the photonic crystal used in our sensor

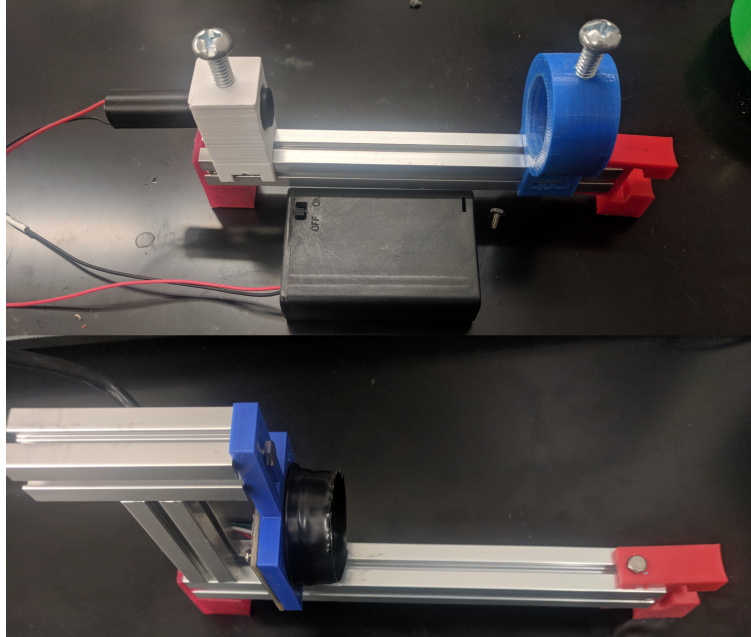


Figure 4: Top: the beam holding the laser and focusing lens. Bottom: the beam holding the camera and neutral density filter.

Each beam is a 15cm x 10mm x 10mm aluminum MakerBeam. Attached on the left side of each beam in Figure

4 is a foot used to keep the beams level with the central platform. On the right side of each beam is a 3D printed connector used to attach the beams to the primary stage. The beams are capable of rotating around the axis that keeps these connectors in place, allowing a larger range of coupling angles for the laser-multilayer system.

The primary stage (see the green 3D printed fixture in Figure 5) acts as the center about which the incident beam can be coupled to the prism and then reflected onto the CCD. The design of this stage allows different types of multilayers to be used since the incident laser can be oriented at nearly any angle. The flowcell stage (see the blue 3D printed piece bolted into the primary stage in Figure 5) is a modular piece that is attached to the primary stage with four bolts. The prism, multilayer, and flowcell chamber are all strapped together on this stage via two pairs of 3D printed braces and hex screws. The modular nature of this piece of the sensor is valuable since multiple designs can be used to achieve the generate BSWs and it only takes between 40 minutes to an hour to print off each flowcell stage.

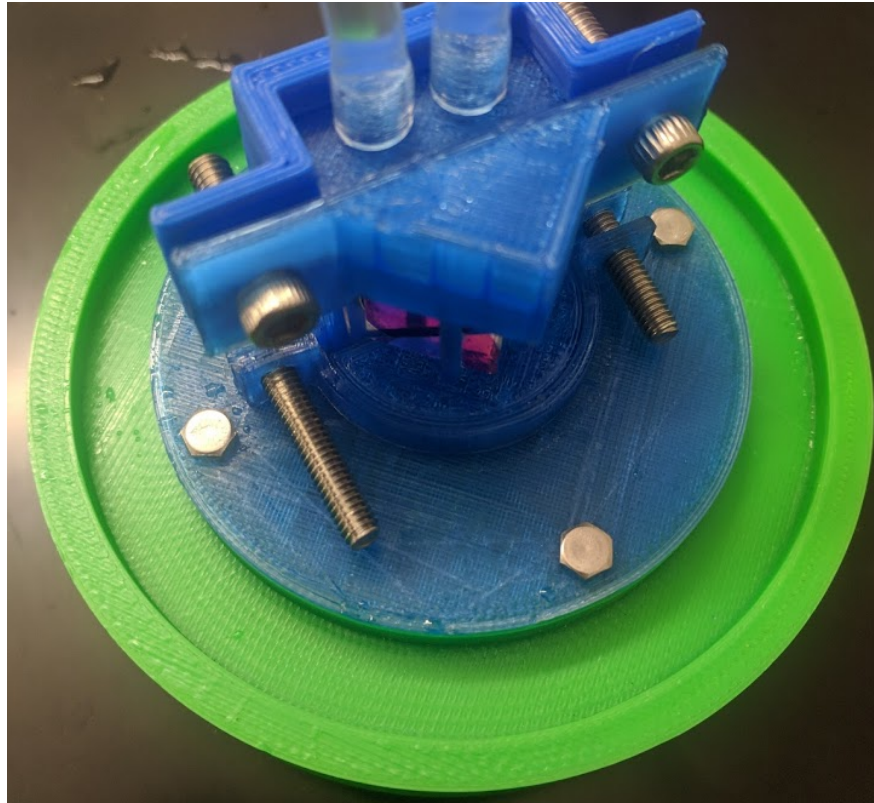


Figure 5: Primary stage and flowcell stage of our sensor. The green round 3D printed fixture underneath the flowcell is the primary stage which the two beams are attached to via a small divot in the back. The blue 3D printed piece mounted to the primary stage is the flowcell stage. The glass prism, multilayer, and flowcell chamber are attached atop the flowcell stage with the use of hex screws and 3D printed braces.

To flow liquids through the chamber the whole fixture must be water tight. To accomplish this we designed the flowcell so that a rubber gasket could be fit around the chamber. When the braces are tightened there is no liquid loss at the interface during operation, however the chamber is made of PLA and liquid will leak through the plastic after a

few hours. The two apertures on top of the flowcell are used for inflow and outflow. To ensure no leaks occur when flushing the chamber we wrapped each aperture with electrical tape before attaching our tubing.

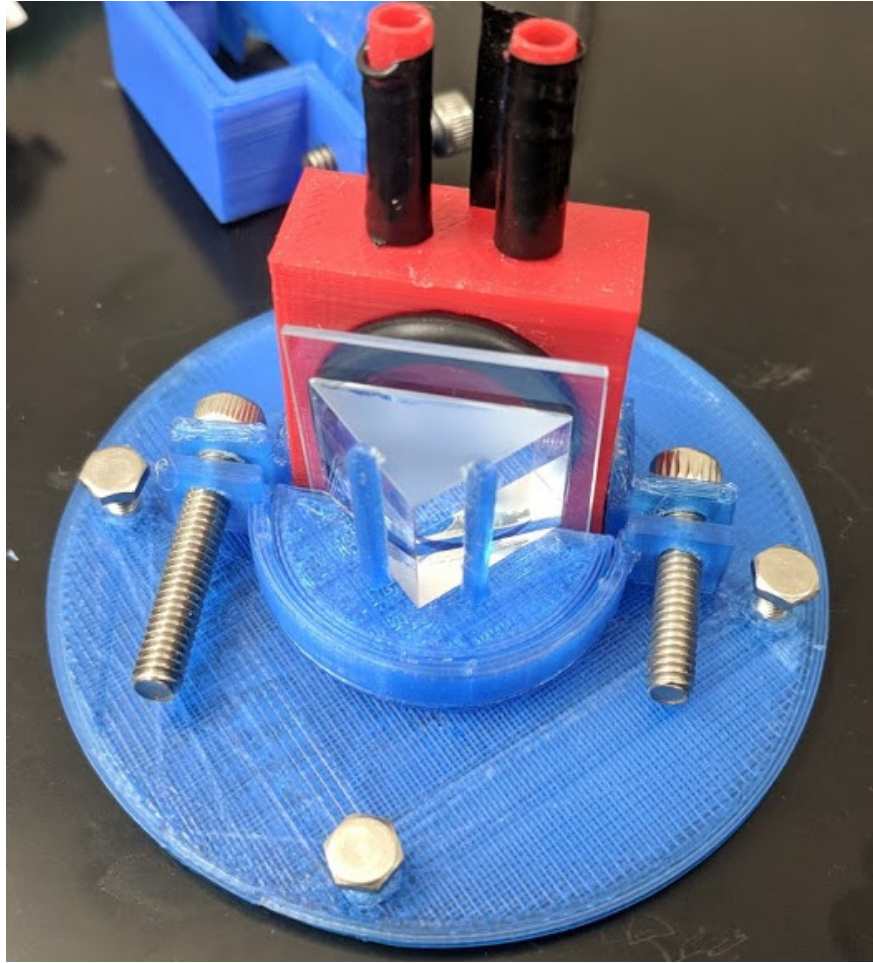


Figure 6: The flowcell stage, prism, multilayer and flowcell chamber. A rubber gasket is set in a groove around the chamber so that when the braces are tightened the interface between the multilayer and flowcell is liquid tight.

The decision to print a flowcell stage separate from the primary stage allows the design to be tinkered with without wasting too much time. Using our 3D printers the primary stage takes about nine hours to print, while the flowcell stage only takes about forty minutes to one hour. This is useful because the position of the glass prism (used to couple incident light to the multilayer) can be more conveniently oriented to produce BSWs. A diagram illustrating the coupling angle required for our multilayer is illustrated in Figure 7. From that diagram it is easy to see how awkward an angle is needed for the sensor to operate, but the ability to translate the prism's bed by printing off another flowcell stage makes it natural to orient the laser at the coupling angle. The next section details how the coupling angle is computed and how data is collected by imaging the surface mode.

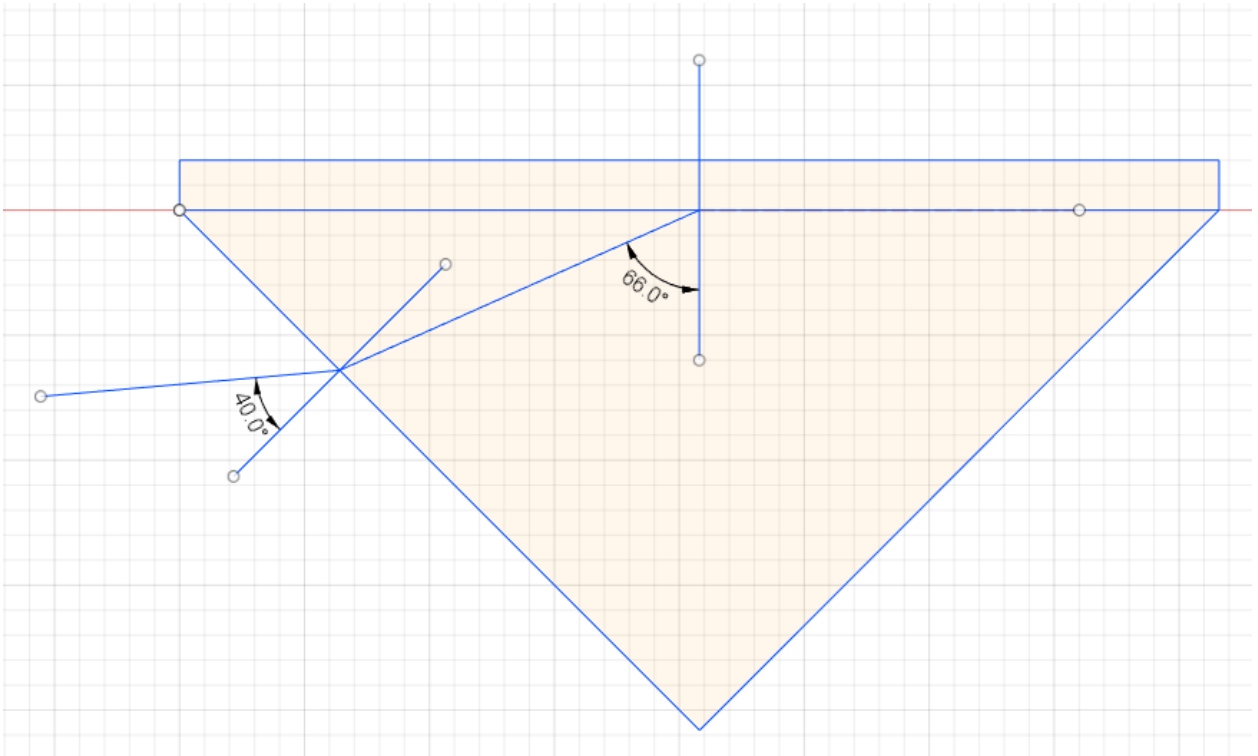


Figure 7: The geometry behind our coupling angle when the flowcell chamber is filled with water. The lines normal to the left leg and hypotenuse of the triangle represent the surface normals of the prism. The line 40.0° from the left leg surface normal and 66° from the hypotenusal surface normal represent the path of the incident light. The laser needs to be oriented about 5° off of parallel with the hypotenusal face of our prism. It is quite an awkward angle, but a different flowcell stage can be printed to make reaching this coupling angle more natural by translating the prism's bed upward.

III. Methods

To image the surface mode and collect data from our biosensor we first prepare the flowcell chamber with the correct substrate or liquid that acts as our reference point for measuring changes in optical properties. After the chamber is prepared we then turn on the beam and rotate it until the coupling angle is reached. Once that angle is reached a dark band representing the angular position of the surface mode will be captured by the CCD. This position occurs at a certain pixel along the horizontal axis of the CCD and serves as the control position of the surface mode.

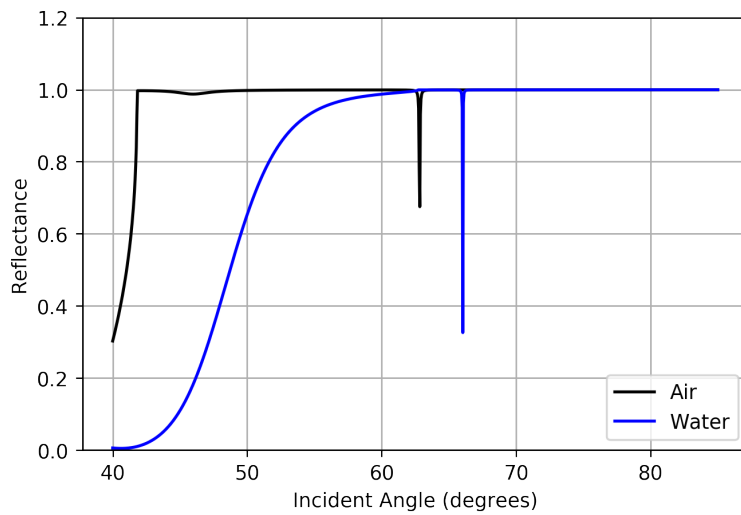
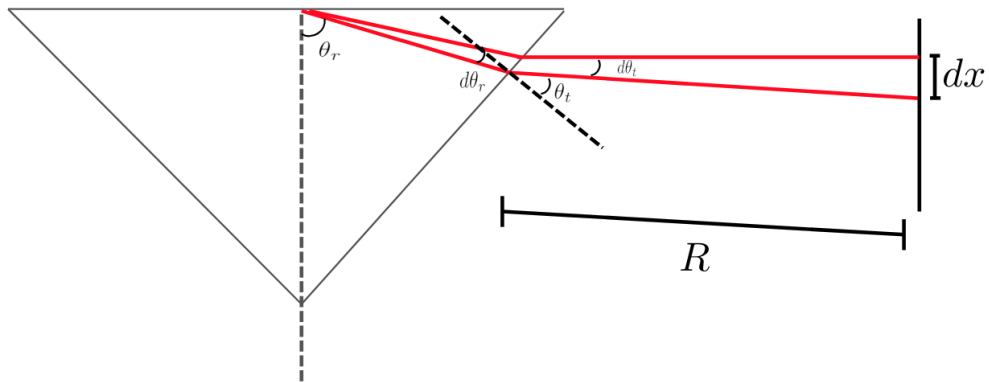


Figure 8: The reflectance characteristic of our multilayer. This plot was developed using a transfer matrix method.

As the index of refraction inside the flowcell chamber changes the dark band will translate left or right from the control position of the surface mode in our reflected image, depending on whether the index is increasing or decreasing. The shift in location of the band, in pixels, corresponds to an angular shift in the part of the reflected beam giving rise to the dark band. This is shown clearly in 8 as we see that a change from an index of 1.00 (air) to 1.33 (water) corresponds to an angular shift of about 3° .

Using the calculated data we can build a model to relate the index of refraction in the chamber to a shift in pixels on our CCD. To construct this relation we require Snell's law and some geometry. Using the classic formula for arclength and the diagram below we find:



$$dx = R d\theta_t$$

Using Snell's law we find

$$\theta_t = \arcsin(\sin(n_g \theta_r))$$

Which implies that

$$d\theta_t = d(\arcsin(n_g \sin \theta_r))$$

$$= \frac{n_g \cos \theta_r}{\sqrt{1 - n_g^2 \sin^2(\theta_r)}} d\theta_r$$

This leaves us with the relation between pixel shift and angular shift:

$$dx = \frac{R n_g \cos \theta_r}{\sqrt{1 - n_g^2 \sin^2(\theta_r)}} d\theta_r \quad (1)$$

Numerically we can determine the relationship between the reflected angle and the index inside the chamber. I wrote a python program to do just that for our multilayer, assuming the chamber is initially filled with water, and a graph of mode position (θ_r) vs index of refraction is plotted in Figure 9.

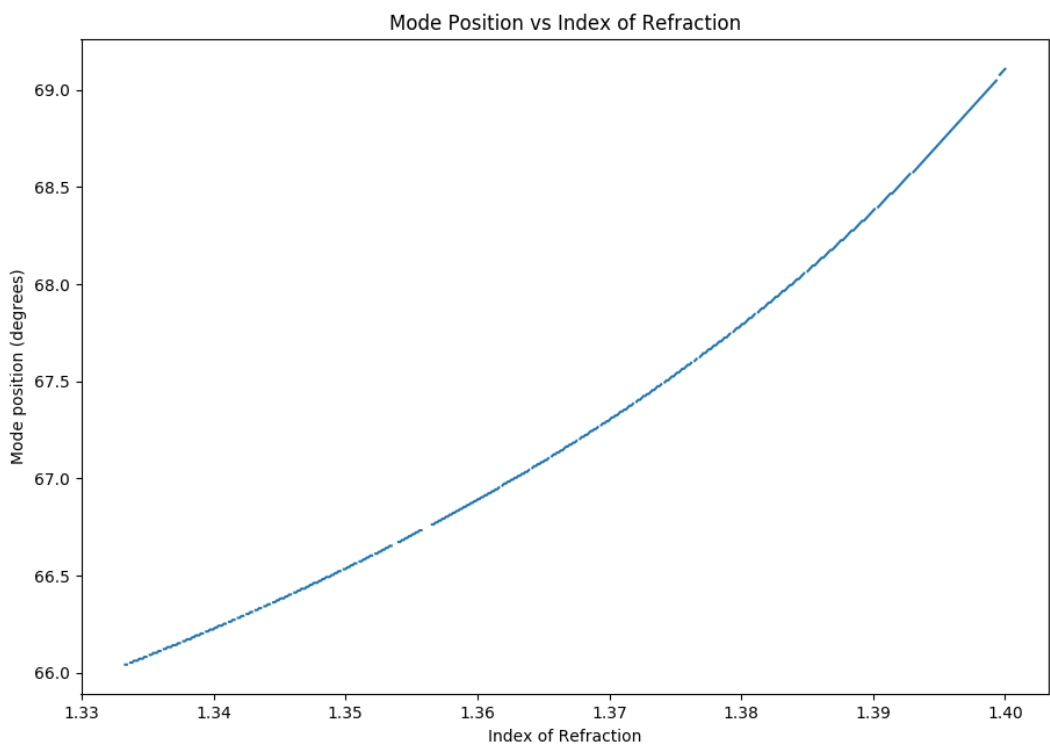


Figure 9: The theoretical relation between the angular position of the mode and the index of refraction inside the flowcell chamber.

IV. RESULTS

The table in Figure 10 lists the mixtures of ethanol used to test for a change in index of refraction. The graph in Figure 10 shows the different indices of refraction corresponding to mixture A being injected over the interval [25, 55]. Similarly mixture B was injected over the interval [70, 90], and mixture C over [100, 150]. After the mixtures have time to settle in the chamber, they are flushed out with the same deionized water used to indicate the baseline mode position. Upon injecting a mixture with a higher index into the chamber we notice that the mode position shifts, as expected. Similar tests for mixtures of acetone and 70% isopropyl alcohol are given in Figures 11 and 12.

Mixtures	A	B	C
Ethanol (ml)	10.0	20.0	30.0
Water (ml)	100.0	100.0	100.0
Index	1.3380	1.3418	1.3450
Pixel Shift	80.0	135.0	245.0
Change in Index	0.0049	0.0052	0.0119

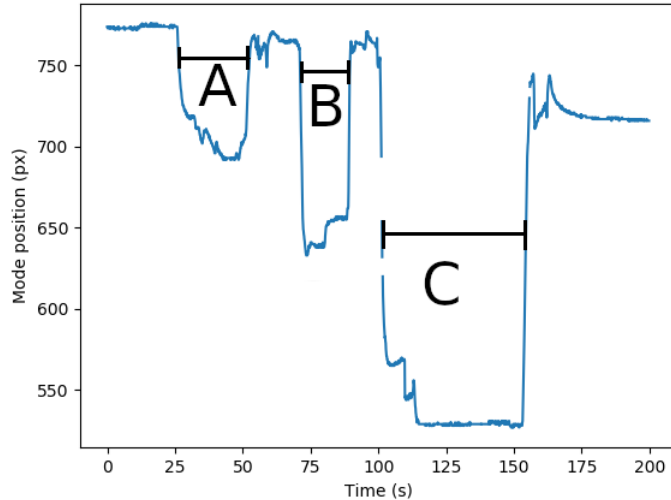


Figure 10: Index shift measurements for ethanol.

Using this data we can acquire a value of an index shift per pixel shift to quantify the sensitivity of the sensor. All of the mixtures used for testing have indices between 1.3380 and 1.3464, meaning that when the pixel shift of each mixture is plotted against the index of each we should expect a linear graph (see Figure 9) since small variations in reflected angle will yield a proportional shift in pixels. By extrapolating the data provided in Figure 13 we find that a shift in one pixel corresponds to a shift of about 0.0018 in index of refraction. This level of sensitivity exceeds the necessary sensitivity to detect surface loading.

Mixtures	A	B	C
Acetone (ml)	10.0	20.0	30.0
Water (ml)	100.0	100.0	100.0
Index	1.3384	1.3430	1.3464
Pixel Shift	111.5	206.0	292.5
Change in Index	0.0052	0.0098	0.0132

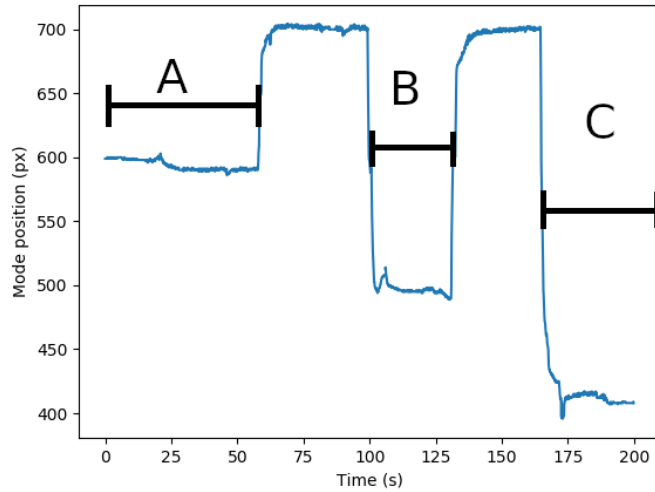


Figure 11: Index shift measurements for acetone.

Mixtures	A	B	C
70% Isop Alc. (ml)	10.0	20.0	30.0
Water (ml)	100.0	100.0	100.0
Index	1.3398	1.3412	1.3447
Pixel Shift	84.5	164.5	223.0
Change in Index	0.0066	0.0080	0.0115

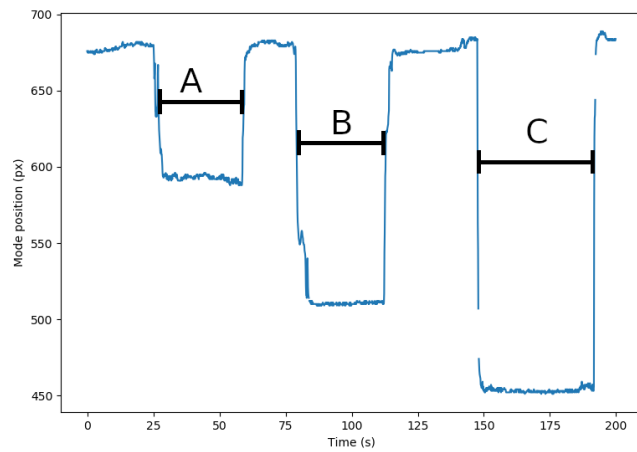


Figure 12: Index shift measurements for 70% isopropyl alcohol.

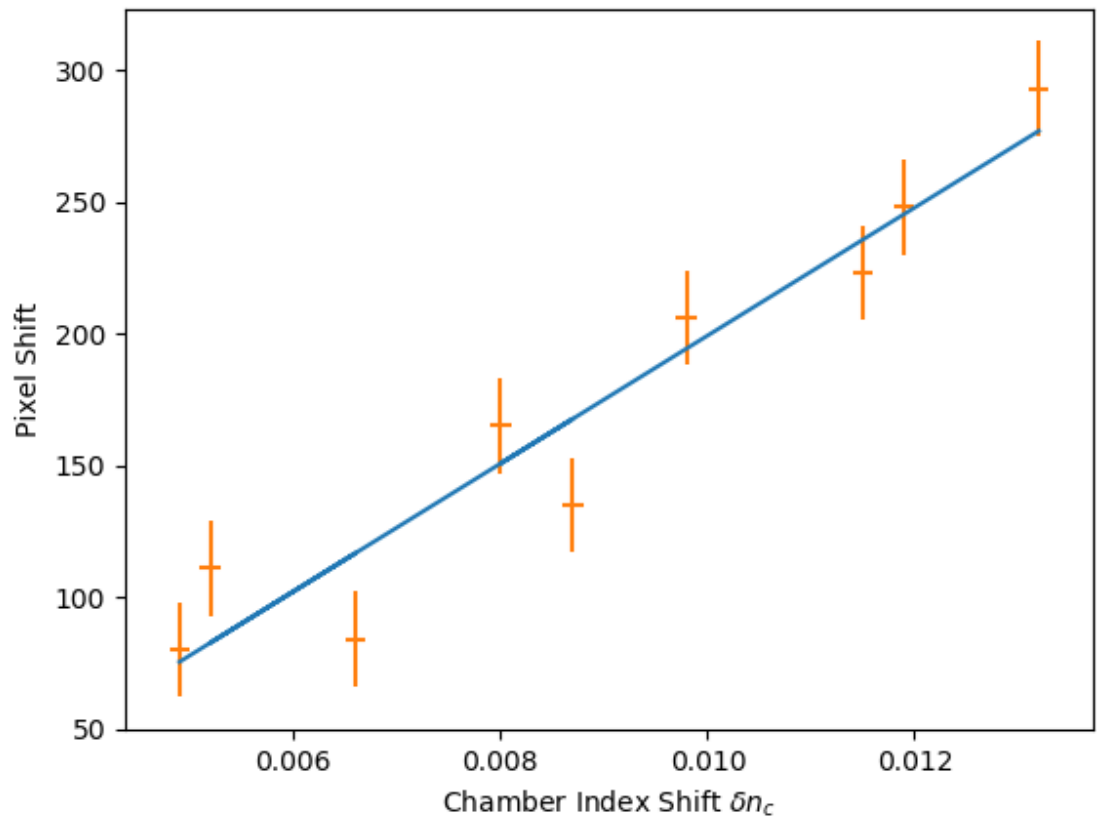


Figure 13: Plotted above is the relationship between a shift in the mode position (measured in pixels) and a shift in the index of refraction of the chamber, δn_c .

V. CONCLUSION

In conclusion, this is a fine alternative to traditional flowcell sensors on the market. The parts that need to be purchased are the multilayers, a low power laser, a focusing lens, a CCD (we took one from a \$40 webcam), and a neutral density filter ($d=3.5$). The rest of the parts can be 3D printed (the CAD files can be found on my GitHub page: <https://github.com/jefferytsummers/thesis>). This sensor offers many advantages over traditional sensors. The synthesis of 3D printed parts and a photonic crystal provide the capability of operation at any wavelength and any incident angle [5]. Users of this sensor can maintain it themselves by cleaning optics, printing off spare parts, and replacing the batteries in the low power laser. The photonic crystal's can be ordered in

The sensor does have a few issues, however. The flowcell itself is not quite water tight. This could be solved by either machining the flowcell or coating the chamber with a water tight sealant. Some multilayers may have coupling angles that are awkward to reach with the current design, however the modular nature of the flowcell stage can aid in reaching the coupling angle. In addition to modifying the flowcell stage, a hemispherical prism could be used in place of the right triangular prism used in our apparatus. The largest uncertainty of our device comes from the error in our ability to measure the pixel shift of the surface mode. At the moment a nine by nine gaussian blur is used to smooth out the image of the surface mode leaving us with an uncertainty in the mode position of about ± 9 pixel. This error can be minimized with respect to our measurements if we move the CCD further away. The error would not be reduced but our measurements of pixel shifts would be much larger than they are with the camera at its current distance.

VI. References

- [1] J. Homola, S. S. Yee, and G. Gauglitz, “Surface plasmon resonance sensors,” *Sensors and Actuators B: Chemical*, vol. 54, no. 1-2, pp. 3–15, 1999.
- [2] W. M. Robertson, “Experimental measurement of the effect of termination on surface electromagnetic waves in one-dimensional photonic bandgap arrays,” *Journal of Lightwave Technology*, vol. 17, no. 11, pp. 2013–2017, 1999.
- [3] J. D. Jackson, *Classical Electrodynamics*. Wiley, 3 ed., 1998.
- [4] D. J. Griffiths, *Introduction to Electrodynamics*. Cambridge University Press, 4 ed., 2017.
- [5] A. Farmer, A. C. Friedli, S. M. Wright, and W. M. Robertson, “Biosensing using surface electromagnetic waves in photonic band gap multilayers,” *Sensors and Actuators B: Chemical*, vol. 173, pp. 79–84, 2012.